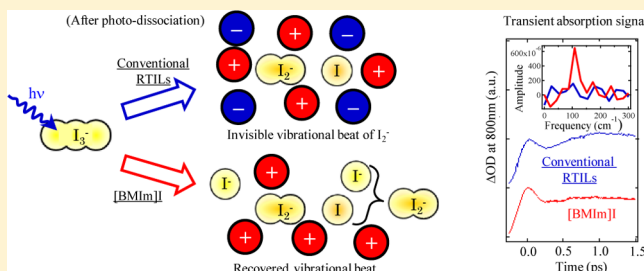


## Ultrafast Relaxation and Reaction of Diiodide Anion after Photodissociation of Triiodide in Room-Temperature Ionic Liquids

Yoshio Nishiyama,<sup>\*,†</sup> Masahide Terazima, and Yoshifumi Kimura<sup>\*,‡</sup>

Department of Chemistry, Graduate School of Science, Kyoto University, Kyoto 606-8502, Japan

**ABSTRACT:** Vibrational dephasing, vibrational relaxation, and rotational relaxation of diiodide ( $I_2^-$ ) after photodissociation of triiodide ( $I_3^-$ ) in room-temperature ionic liquids (RTILs) were investigated by ultrafast transient absorption spectroscopy. The vibrational energy relaxation (VER) rate of  $I_2^-$  produced by the photodissociation reaction of  $I_3^-$  was determined from the spectral profile of the transient absorption. The rates in RTILs were slightly slower than those in conventional liquids. On the other hand, the coherent vibration of  $I_2^-$  was not observed in RTILs, and the vibrational dephasing of the photoproducted  $I_2^-$  was accelerated. This was explained by the interaction between  $I_2^-$  and I consisting of a caged contact pair in RTILs. The orientational relaxation time of  $I_2^-$  determined by the transient absorption anisotropy was much longer in RTILs than in conventional liquids due to their high viscosities although the relaxation time was shorter than the prediction from the Stokes–Einstein–Debye (SED) theory. The deviation from the SED prediction was interpreted by the frequency dependence of the shear stress acting on the molecule. The dynamics of  $I_2^-$  in 1-butyl-3-methylimidazolium iodide ([BMIm]I) were quite different from those in other conventional RTILs: the coherent vibration of  $I_2^-$  was observed for the time profile of the transient absorption and the initial value of the anisotropy was reduced to 0.31 from 0.36 in conventional RTILs. These results suggest that an ultrafast reaction between the photofragment I and the solvent  $I^-$  may occur during the photodissociation process of  $I_3^-$ . The anomaly in the ground state coherent vibration and steady state Raman spectrum of  $I_3^-$  also suggest the possibility that  $I_3^-$  and  $I^-$  can be located in vicinity and interact strongly with each other in [BMIm]I.



## 1. INTRODUCTION

Transport properties of room-temperature ionic liquids (RTILs) have attracted a lot of attention mostly for their application to the electrochemical field.<sup>1–6</sup> Interestingly, several ions have been reported to show anomalous transport properties in RTILs.<sup>5,6</sup> For example, Kawano et al. reported that the conductivity of the  $I_3^-/I^-$  system, which is used as a redox couple of dye-sensitized-solar-cells,<sup>7</sup> dramatically increases in RTILs with increasing the concentration of  $I_3^-$  and  $I^-$ .<sup>6</sup> They suggested that the Grotthuss-like exchange reaction ( $I_3^- + I^- \rightarrow I^- \cdots I_2^- \cdots I^- \rightarrow I^- + I_3^-$ ) may enhance the diffusion of  $I_3^-$  and  $I^-$ . Another group applied Raman spectroscopy for the similar system and found that a new vibration band assigned to  $I_5^-$  appears under the high concentration of  $I_3^-$  and  $I^-$ .<sup>8</sup> This result indicates the possibility that polyiodide may contribute to the charge transport, e.g.,  $I_5^- + I^- \rightarrow I_3^- + I_3^- \rightarrow I^- + I_5^-$ .

With relation to these phenomena, the reaction dynamics of iodide, diiodide, and triiodide are quite interesting, and several spectroscopic measurements have been applied to these species. Takahashi et al. observed the bimolecular reaction between diiodide anion radicals ( $I_2^- + I_2^- \rightarrow I_3^- + I^-$ ) in several RTILs by transient absorption measurement, and found that the reaction rate is slightly faster than that predicted from a simple diffusion-limited reaction model (Smoluchowski theory) using the diffusion coefficient of  $I_2^-$  calculated from the Stokes–Einstein (SE) relation.<sup>9</sup> Later, we determined the diffusion coefficients of  $I_2^-$  in RTILs experimentally by the transient grating spectroscopy

and concluded that the charge of the reactant ion is almost thoroughly screened by surrounding solvent ions consisting of RTILs, and that the reaction dynamics is well modeled by the Smoluchowski theory without the charge interaction between reactants.<sup>10</sup> A similar screening effect may also play an important role in the diffusive encounter between other polyiodide such as  $I_3^-$  and  $I^-$ .

Triiodide photodissociation ( $I_3^- + h\nu \rightarrow I_2^- + I$ ) is also an important photoreaction to elucidate the dynamics of triiodide and the related species. Ultrafast spectroscopy has been applied for this reaction system in recent decades, and several elementary processes have been reported in polar solvents:<sup>11–14</sup>

not only the dissociating process, but also recombination, energy dissipation and coherent process of the fragment. After the photoexcitation,  $I_3^-$  is brought into the dissociative state, where  $I_3^-$  is separated into  $I_2^-$  and I in a few hundred femtoseconds.<sup>11a,12a,c</sup> Since this bond cleavage produces the photofragments impulsively, the temporal absorption of  $I_2^-$  around 800 nm shows a quantum beat (a period of 300 fs) for about 1 ps.<sup>11a,b,12a</sup> In addition, the photoproducted  $I_2^-$  has a significant amount of excess vibrational energy, which will be released to the solvent. This process has been monitored by the absorption spectral change of  $I_2^-$ , and the vibrational energy relaxation (VER)

Received: December 21, 2011

Revised: March 30, 2012

Published: June 13, 2012

time is estimated to be about several picoseconds,<sup>11a,b,12a</sup> which is much faster than that of  $I_2^-$  (ca. 200 ps).<sup>15</sup> The VER of  $I_2^-$  was also investigated through photodissociation reaction of  $I_2^-$  ( $I_2^- + h\nu \rightarrow I^- + I$ ), where a hot  $I_2^-$  molecule is produced by the fast geminate recombination of the fragments ( $I^- + I \rightarrow I_2^-$ ).<sup>16a-c</sup> This study revealed that the energy dissipation shows a nonexponential character: the quanta at the higher level relax into the low level of  $v = 1$  or 2 very rapidly (in subpicoseconds), and the subsequent relaxation occurs slowly. The recombination between  $I_2^-$  and  $I$  occurs within a few hundred picoseconds by the cage effect of solvent. Ruhman's group evaluated the escape probability of the fragments from the absorption intensity of  $I_2^-$  at the long time (ca. 400 ps) in various solvents and reported that the geminate recombination process depends mainly on the solvent viscosity.<sup>11d,e</sup> Later, they also found a new absorption band, which is red-shifted compared with that of normal  $I_2^-$ .<sup>11f</sup> This new band is assigned with the absorption of a caged contact pair [ $I_2^- \cdots I$ ], i.e., adjacent  $I_2^-$  and  $I$  in the solvent cage.

We have recently reported the recombination dynamics of photofragments after the photodissociation of  $I_3^-$  in RTILs using ultrafast transient absorption spectroscopy.<sup>17</sup> It was found that all of the fragments exist as the caged contact pair in RTILs and that they recombine geminately with the time constant of 60 ps. On the other hand, free  $I_2^-$  molecules escaped from the cage were observed exceptionally in 1-butyl-3-methylimidazolium iodide, [BMIm]I. We considered that a free  $I_2^-$  molecule is produced by an additional reaction between photofragment  $I$  and solvent anion  $I^-$  ( $I + I^- \rightarrow I_2^-$ ).

In this study, we have investigated ultrafast relaxation dynamics of  $I_2^-$  after the photodissociation of  $I_3^-$  in RTILs such as VER, rotational relaxation, and vibrational dephasing. In the following section, experimental details will be presented. In section 3, a model required for the spectroscopic calculation will be briefly explained. Results and discussion will be shown in section 4. It will be shown that vibrational dephasing process is accelerated in RTILs, and coherent vibration of  $I_2^-$  cannot be observed. On the other hand, the vibrational relaxation in RTILs is found to be somewhat slower than those in conventional liquids. For [BMIm]I, dephasing of  $I_2^-$  vibration and initial reorientational dynamics of  $I_2^-$  are different from those in other RTILs. The uniqueness of this liquid will be explained by the reaction with the solvent  $I^-$ .

## 2. EXPERIMENTAL METHOD

The transient absorption measurement was carried out using a portion of output from an amplified Ti:Sapphire laser system (Spectra Physics, Tsunami & Spitfire ProXP, 800 nm, 1.9 W, 120 fs, 1 kHz). The pump pulse (400 nm) was obtained by doubling the fundamental light in 0.5 mm LBO crystal. For a probe pulse, we used the remaining fundamental pulse or white light continuum generated by focusing the fundamental pulse into a 2 mm sapphire plate. The desired wavelength out of the white light was selected using a 10 nm bandpass filter (Semrock Inc.). In several experiments, a portion of 400 nm excitation pulse was also used as the probe pulse for monitoring the ground-state dynamics of  $I_3^-$ . A portion of the probe pulse was separated by a beam splitter and used as a reference pulse for correcting the fluctuation of the pulse intensity. The pump and the probe pulses were overlapped spatially at a sample cell of 1 mm path length with a lens of a focal length of 200 mm, and the pump pulse was loosely focused so that the spot size of probe pulse was smaller than that of the pump pulse. The

polarization of the probe pulse was rotated to the magic angle to that of the pump pulse by a half wave plate except for transient anisotropy measurement. The pulse energies of the pump and probe pulses were typically 1  $\mu$ J and 20 nJ, respectively. The intensities of the probe and the reference pulses were monitored by Si photodiodes (Hamamatsu Photonics) and accumulated by a Boxcar integrator (Stanford Research System, Inc.). The difference of the optical density ( $\Delta OD$ ) with and without the pump pulse at each delay time was obtained by a toggle mode using an optical chopper, and the fluctuation of the intensity of the probe pulse was corrected by the intensity of the reference pulse. The average was taken over 4000 pulses at each delay time. The time zero at each wavelength was determined by the optical Kerr signal of neat acetonitrile measured under the same experimental condition. In the transient anisotropy measurement, the polarization of the probe pulse was set to 45° against that of pump pulse. The probe pulse after passing through the sample solution was separated into the parallel and the perpendicular components against the polarization of the pump pulse by a polarizer. From  $\Delta OD$  at each polarization (parallel  $\parallel$  and perpendicular  $\perp$ ), we calculated the anisotropy  $r_{\Delta OD}(t)$  by the following equation:

$$r_{\Delta OD}(t) = \frac{\Delta OD(t)_{\parallel} - \Delta OD(t)_{\perp}}{\Delta OD(t)_{\parallel} + 2\Delta OD(t)_{\perp}} \quad (1)$$

RTILs used in this study were 1-butyl-3-methylimidazolium hexafluorophosphate ([BMIm][PF<sub>6</sub>]), BMIm bis(trifluoromethanesulfonyl)amide ([BMIm][NTf<sub>2</sub>]), BMIm iodide ([BMIm]I), and *N,N,N*-trimethyl-*N*-propylammonium NTf<sub>2</sub> ([N<sub>1,1,1,3</sub>][NTf<sub>2</sub>]). These were used after evacuation using a vacuum line for more than 2 h at 323 K. Molecular solvents such as methanol, ethanol, 1-propanol, water, acetonitrile (spectroscopic grade) and glycerol triacetate (GTA) (guaranteed grade) were used without further purification. The triiodide solution was produced by dissolving potassium iodide and iodine crystal in solvent, of which absorbance was adjusted to be 0.3 at 400 nm for 1 mm optical path. In the case of [BMIm]I, it was found that there is an absorption band in the wavelength region corresponding to the absorption of triiodide without dissolving iodine (absorbance is 1.4 for 1 mm optical path). The triiodide is considered to be produced from iodide through unknown reactions of  $I^-$ . Therefore, we used [BMIm]I without dissolving iodine and potassium iodide. All solutions were filtered before the spectroscopic measurement in order to remove undissolved solute or dust. Viscosities of RTILs except [BMIm]I (shown in Table 2) were measured using a viscometer (Brookfield LVDV-II, cone plate CPE-40) at 298 K. Raman spectra of the solution were measured by using a 532 nm CW laser as a light source, and the experimental setup is the same as the previous studies except for the laser source.<sup>18</sup>

## 3. ANALYTICAL EXPRESSION OF THE ABSORPTION INTENSITY OF $I_2^-$

We probed mainly the absorption band of  $I_2^-$  around 800 nm in this study. This band corresponds to the transition from the ground state ( $^2\Sigma_u$ ) to the first excited state ( $^2\Pi_g$ ).<sup>19</sup> These electronic states were modeled by the following Morse potential and an exponential-typed one, respectively (Figure 1).<sup>19</sup>

$$V_g(R) = D_e \{ [\exp(-aR) - 1]^2 - 1 \} \quad (2)$$

$$V_e(R) = A \exp(-R/\alpha) \quad (3)$$

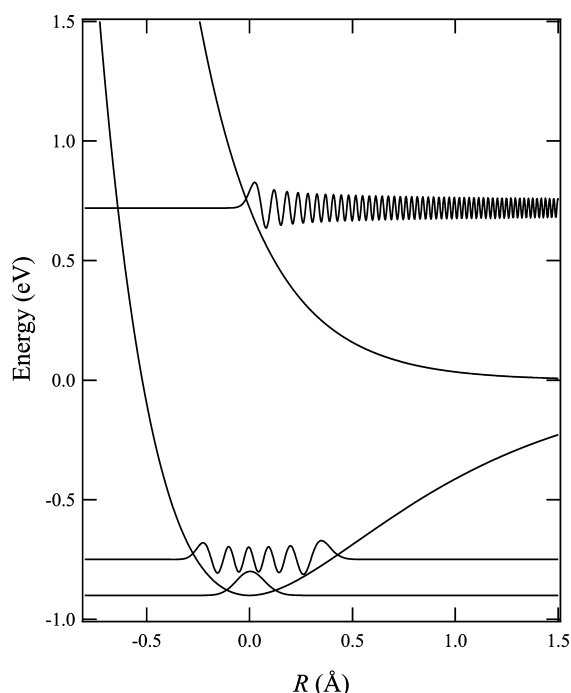


**Figure 1.** Potential curves of the electronic ground and excited state calculated with the parameters in the case of [BMIm][NTf<sub>2</sub>]. The wave functions of  $\nu = 0$  and 10 in the ground state and  $E = 0.72$  eV in the excited state are also shown.

where  $R$  is the displacement of internuclear distance between iodine atoms from the equilibrium distance.  $D_e$ ,  $A$ ,  $a$ , and  $\alpha$  represent the dissociation energy of  $I_2^-$ , the repulsive potential parameter in the excited state, and the distance parameters for the ground and the excited states, respectively. The harmonic frequency  $\omega$  and anharmonicity  $\chi_e$  in the electronic ground state are given by  $D_e$  and  $a$ .

For the calculation of the absorption spectrum, a Franck–Condon factor is required. As shown in Figure 1, the nuclear wave function in the electronic excited state decays to zero right outside the potential and oscillates rapidly inside. Therefore, it is approximately considered that the transition from a bound state to a continuum state occurs only at the classical turning point of the excited state.<sup>20–23</sup> Assuming the transition moment independent of the nuclear distance in addition to the above approximations, the absorption spectrum  $I(\lambda, t)$  is described by the “reflection principle” as follows:

$$I(\lambda, t) \propto \frac{1}{\lambda} \sum_{\nu} P_{\nu}(t) |\Psi(\mathbf{v}, R_{\nu, \lambda})|^2 \quad (4)$$

where  $P_{\nu}(t)$  is the population of vibrational level  $\nu$  at time  $t$ , and  $\Psi(\mathbf{v}, R_{\nu, \lambda})$  is the ground state wave function at the position ( $R_{\nu, \lambda}$ ) where the transition occurs, respectively. The value of  $R_{\nu, \lambda}$  is described by

$$R_{\nu, \lambda} = -a \ln \{ [2\pi\hbar c/\lambda - D + \hbar(\omega(\nu + 1/2) - \chi_e(\nu + 1/2)^2)]/A \} \quad (5)$$

In the calculation of the transient absorption spectrum, we first determined potential parameters in each solvent by fitting the absorption spectrum of steady-state  $I_2^-$  with eqs 4 and 5, by assuming that  $P_{\nu}(t)$  follows the Boltzmann distribution. As the steady state absorption spectrum, we used the data at 20 ps because the VER times in conventional liquids have been

reported to be more or less several picoseconds<sup>11a,b,12a,16a–c</sup> and because spectra in RTILs did not change after 10 ps.<sup>17</sup> In the spectral fitting,  $\omega$  was fixed to 115 cm<sup>−1</sup>, which was the value reported for  $I_2^-$  vibration in conventional liquids,<sup>24</sup> and the vibrational states to  $\nu = 20$  were counted. The parameters ( $A$ ,  $\alpha$ ,  $D$ , and  $\chi_e$ ) obtained by the fit are listed in Table 1.

**Table 1.** The Parameters on the Electronic Excited Potential and Temporal Vibrational Energy

solvent	$A$ (eV)	$\alpha$ (Å)	$D$ (eV)	$\chi_e$	$\tau_{\text{VER}}$ (ps)
acetonitrile	0.72	0.33	0.87	1.3	2.5
methanol	0.72	0.31	0.85	2.5	2.3
ethanol	0.72	0.32	0.86	1.4	2.3
1-propanol	0.72	0.31	0.87	2.1	2.6
water	0.72	0.3	0.88	2.3	1.8
[BMIm][NTf <sub>2</sub> ]	0.72	0.28	0.87	0.5	3.3
[BMIm][PF <sub>6</sub> ]	0.72	0.27	0.85	1.0	2.9
[N <sub>1,1,1,3</sub> ][NTf <sub>2</sub> ]	0.72	0.27	0.85	0.5	2.8
GTA	0.72	0.26	0.86	0.6	3.1

## 4. RESULT AND DISCUSSION

**4.1. VER and Fast Recombination.** Figure 2a shows the time profiles of transient absorption signals in [BMIm][NTf<sub>2</sub>] probed at various wavelengths. Similar to the previous studies in the conventional liquids, the transients in RTILs also showed wavelength-dependent dynamics in the initial several picoseconds,<sup>11a–f,12a</sup> e.g., the time profiles at 700 and 970 nm decayed much faster than others. This behavior corresponds to the change of the spectral shape due to VER as shown in the transient absorption spectra reconstructed from each time profile (Figure 2b). In addition, the integrated absorption intensity decreased temporally in this time range. These results indicate that both the VER and the geminate recombination occur in RTILs at this earlier time scale.

In order to obtain the transient vibrational distribution of  $I_2^-$ ,  $P_{\nu}(t)$ , we tried to fit the time-resolved spectra based on eqs 4 and 5 using the potential parameters in Table 1. In the fitting, it was difficult to determine  $P_{\nu}(t)$  for each level independently, because more than 10 vibrational levels can contribute to the absorption intensity and because the signal-to-noise ratio (S/N) of the transient absorption spectra was not enough.<sup>12a</sup> Instead, we used a model function with a few parameters for describing the population distribution as

$$P_{\nu}(t) = (\nu - \mu)^{\gamma(t)-1} \frac{e^{-(\nu-\mu)/\theta(t)}}{\Gamma(\gamma)\theta(t)^{\gamma(t)}} \quad (6)$$

where  $\Gamma(\gamma)$  is the gamma function, and  $\mu(t)$ ,  $\theta(t)$ , and  $\gamma(t)$  are the parameters depending on the delay time. We first examined whether this function can represent the distribution based on the possible physical process. The following Master equation was often used in order to describe the vibrational distribution during VER:<sup>11b,13c</sup>

$$\begin{aligned} \frac{dP_{\nu}(t)}{dt} = & ((\nu + 1)kP_{\nu+1}(t) - (\nu + 1)k^{-1}P_{\nu}(t)) \\ & - (\nu kP_{\nu}(t) - \nu k^{-1}P_{\nu-1}(t)) \end{aligned} \quad (7)$$

$$k^{-1} = k \exp(-\hbar\omega/k_{\text{B}}T) \quad (8)$$

where  $k$  and  $k^{-1}$  are the relaxation rate from  $\nu = 1$  to  $\nu = 0$  and vice versa, and the transition rate at each vibrational quantum is

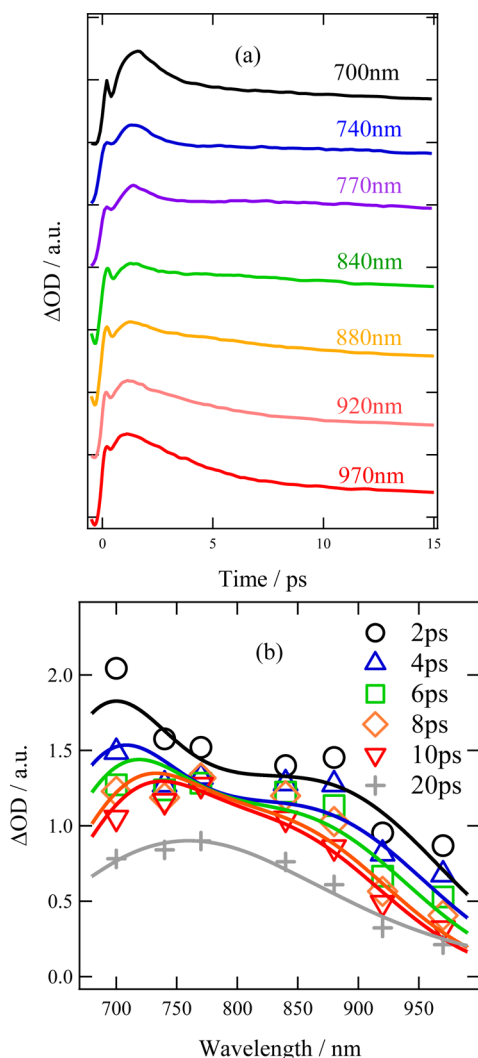


**Figure 2.** (a) Time profiles of the transient absorption signals at several wavelengths in [BMIm][NTf<sub>2</sub>]. Each time profile has a different vertical offset for clarity. (b) Transient absorption spectra in [BMIm][NTf<sub>2</sub>] at several delay times. Solid lines represent the calculated curves whose detail is described in section 4.1.

assumed to increase in proportion to the vibrational quantum number. Numerical solutions of  $P_v(t)$  of eq 7 starting from  $P_v(t) = 1$  for  $v = 40$  was simulated by eq 6. The results of the fit together with the numerical solution of  $P_v(t)$  are shown in Figure 3. As is shown in Figure 3, the model function reasonably represents the numerical solution. Therefore, we carried out the fitting of the spectrum at each delay time with  $\mu(t)$ ,  $\theta(t)$  and  $\gamma(t)$  as parameters using eqs 4–6. Typical examples of the fitting at several delay times are shown by the solid line in Figure 2b. As is shown in the figure, the fitting curves represent the spectra at the longer delay time than a few picoseconds well, whereas the deviation from the experimental results became larger as the delay time is earlier. This is considered to be mainly due to the limitation of the simple modeling for the electronic potentials and vibrational distribution. Therefore, we will discuss the excess energy dissipation for the data after a few picoseconds hereafter. The population distribution  $P_v(t)$  at each delay was obtained from the fitting parameters  $\mu(t)$ ,  $\theta(t)$ , and  $\gamma(t)$ , and the examples are shown in Figure 4a. The profiles are similar to those reported in the previous studies.<sup>11b,12a,13c</sup>

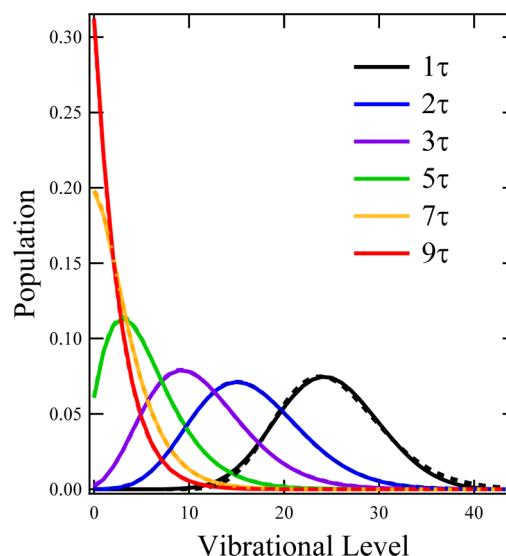


**Figure 3.** The population distribution at several delay times shown in ref 11b (dotted curve) and the fitting result of it with gamma distribution (solid curve). The delay times are normalized by  $\tau = 2.32k$  where  $k$  is identical with that in eqs 7 and 8.

The time profile of averaged vibrational energy,  $\bar{E}_{\text{vib}}$  was calculated for each solvent by

$$\bar{E}_{\text{vib}}(t) = \sum_v P_v(t) (v + 1/2) \hbar \omega = \Delta E(t) + E_{\infty} \quad (9)$$

where  $\Delta E(t)$  is the vibrational excess energy (shown in Figure 4b). The time profile of  $\Delta E(t)$  was well simulated by a single exponential function as follows:

$$\Delta E(t) = \Delta E(0) \exp(-t/\tau_{\text{vib}}) \quad (10)$$

where  $\tau_{\text{vib}}$  is the VER time. The parameters obtained by the fit are listed in Table 1 for all solvents except for [BMIm]I. We excluded the result for [BMIm]I from the fit since other photochemical dynamics occurs in this RTIL as will be described later. The relaxation times  $\tau_{\text{vib}}$  in conventional solvents are similar to those in the previous studies.<sup>11b,12a,13a</sup> When we compare the values of  $\tau_{\text{vib}}$  between in RTILs and nonionic solvents, the result of RTILs are found to be similar to or slightly longer. Considering that the VER rate is related with the friction acted on the intended vibrational motion  $\xi(\omega)$  as shown in the Landau–Teller formula ( $\tau_{\text{vib}} = k_B T / \xi(\omega)$ ),<sup>25</sup> this result means that the vibrational friction is not enhanced in RTILs despite the Coulomb interaction between solute  $\text{I}_2^-$  and solvent ions.

Our results are similar to previous experimental observations using the time-resolved IR for three negative ions,  $\text{N}_3^-$ ,  $\text{NCS}^-$ , and  $\text{N}(\text{CN})_2^-$ ;<sup>26,27</sup> the VER rates of the antisymmetric bands around 2000  $\text{cm}^{-1}$  are similar to those in less polar aprotic solvents and slower than in protic solvents. The slow VER was attributed to the weak hydrogen bonding between the probed ions and RTILs based on the correlation between the VER rate and the peak shift of the static IR spectrum. In the present case, however, the vibrational frequency of  $\text{I}_2^-$  (115  $\text{cm}^{-1}$ ) is much lower than the above case (ca. 2000  $\text{cm}^{-1}$ ), and the mechanism of the VER should be different from previous examples. In the low frequency region, VER is not so sensitive to the specific interaction such as hydrogen bonding, since the low frequency vibrational motion is perturbed by various low frequency motions such as libration, rotation and translation of solvent.



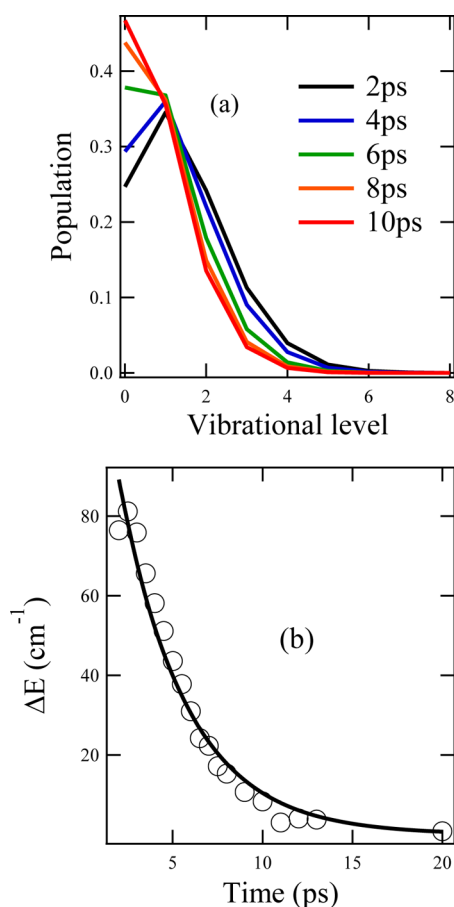


**Figure 4.** (a) Population distributions at several time delays in [BMIm][NTf<sub>2</sub>] obtained from the spectral fitting. (b) Time profile of averaged vibrational energy in [BMIm][NTf<sub>2</sub>]. Solid line represents the fitting curve by single exponential function.

Kim et al. investigated the VER of the lower frequency mode (vibration of polar diatomic molecule of the frequency of about 600 cm<sup>-1</sup>) in RTILs and conventional liquids.<sup>28</sup> They calculated not only the VER rates but also the power spectrum of  $\xi(\omega)$ , which represents the dependence of VER rate on the vibrational frequency, in the range of 0 to 800 cm<sup>-1</sup> (Figure 7d in ref 28). According to their result, the value of  $\xi(\omega)$  in [EMIm][PF<sub>6</sub>] is smaller than those in water and acetonitrile in the low frequency region (below 150 cm<sup>-1</sup>). This is consistent with our result, although the model molecule in the calculation does not have a charge. Therefore, the solvent structure or dynamics of RTILs themselves are considered to be important in determining the VER rate in RTILs.

The theoretical studies indicated that VER at low frequency is determined mainly by collisional force rather than Coulomb force.<sup>29–33</sup> the attractive electrostatic force causes the acceleration of VER mainly by increasing the local density of solvent molecules around a solute.<sup>13a,30</sup> For RTILs, the local density enhancement of solvent cations around I<sub>2</sub><sup>-</sup> is expected to be large due to the strong charge–charge attraction. However, solvent number density in bulk RTIL (about 5M) is smaller than conventional liquids (more than 10M). Therefore, the effect of local density enhancement of solvent ions in RTILs may be canceled.

**4.2. Anisotropy Measurement: Reorientation of I<sub>2</sub><sup>-</sup>.** Transient anisotropy decays of I<sub>2</sub><sup>-</sup> in ethanol, [BMIm][NTf<sub>2</sub>], and [BMIm]I are shown in Figure 5. The initial values

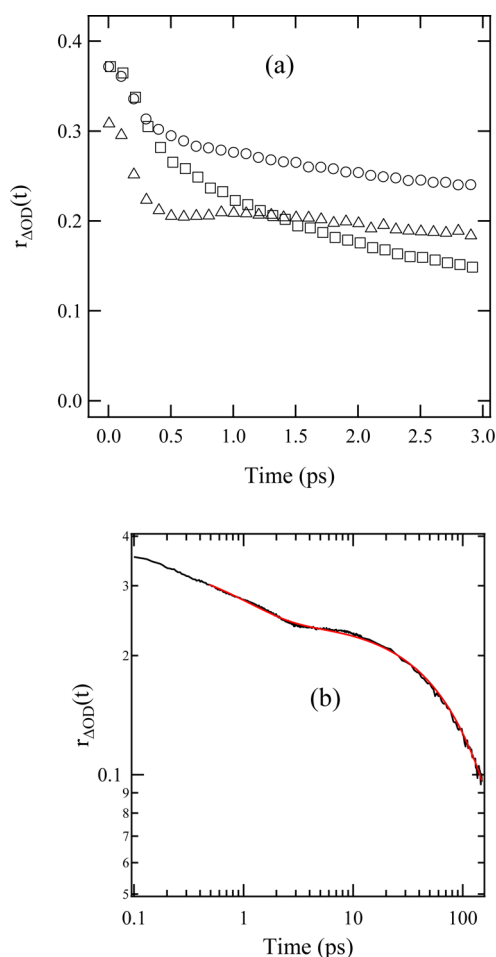


**Figure 5.** (a) Time profiles of transient anisotropy probed at 800 nm: ○ [BMIm][NTf<sub>2</sub>], □ [BMIm]I, △ ethanol. (b) Time profiles of transient anisotropy probed at 800 nm in [BMIm][NTf<sub>2</sub>]. The horizontal and vertical axes are logarithmic. Red line is a fitting curve by eq 11.

( $r_{\Delta OD}(0)$ ) are nearly 0.36 in all solvents except for [BMIm]I (see Table 2). The value close to 0.4 is reasonable, because the

**Table 2. Amplitudes and Time Constants of Anisotropy Decay in Various Solvents**

solvent	$r_{\Delta OD}(0)$	$\tau_f$ (ps)	$\tau_s$ (ps)	$\beta$	$\langle \tau_{ave} \rangle$ (ps)	$\eta$ (cP)
acetonitrile	0.34	1.2	3.0	1	3.0	0.3
methanol	0.36	1.1	5.3	1	5.3	0.55
ethanol	0.36	1.2	6.7	1	6.7	1.0
1-propanol	0.36	1.0	10	1	10	2.2
water	0.36	0.9	6.2	1	6.2	0.9
[BMIm][NTf <sub>2</sub> ]	0.36	1.0	150	0.7	200	52
[BMIm][PF <sub>6</sub> ]	0.36	1.2	320	0.79	370	270
[BMIm]I	0.31	1.5	200	0.5	500	1800
[N <sub>1,1,1,3</sub> ][NTf <sub>2</sub> ]	0.37	1.4	198	0.65	280	72
GTA	0.37	1.5	97	0.9	102	17

transition dipole moments of both I<sub>3</sub><sup>-</sup> and I<sub>2</sub><sup>-</sup> are parallel to their molecular axes. The smaller value in [BMIm]I may be originated from the additional I<sub>2</sub><sup>-</sup> created by the reaction of I with the solvent ion, which will be described later.

In a few hundred femtoseconds,  $r_{\Delta OD}(t)$  is almost independent of the solvent in contrast to the solvent dependent dynamics of  $r_{\Delta OD}(t)$  in the longer time scale. The similarity in

the initial dynamics can be understood considering that the inertial rotation of  $I_2^-$  is predominant in a few hundred femtoseconds. In the longer time scale, rotational diffusion contributes dominantly to the decay, and the transients are solvent-dependent. Since the diffusive motion was very slow for RTILs with high viscosities, it was difficult to measure  $r_{\Delta OD}(t)$  until it reached zero because of the short lifetime of  $I_2^-$  (ca. 60 ps). Therefore the longer dynamics of  $r_{\Delta OD}(t)$  was analyzed within this limitation. The decay was deviated from a single exponential behavior in RTILs in a longer delay time region as reported for other dyes measured by fluorescence anisotropy. The decay of  $r_{\Delta OD}(t)$  in the longer time scale after 0.5 ps was simulated by the combination of a single exponential function and a stretched exponential function as follows:

$$r_{\Delta OD}(t) = A_{\text{fast}} \exp(-t/\tau_f^r) + A_{\text{slow}} \exp(-(t/\tau_s^r)^\beta) \quad (11)$$

where  $\tau_f^r \ll \tau_s^r$ . The smaller value of  $\beta$  less than 1 represents a broad distribution of rotational relaxation time due to the inhomogeneous solvent environment.<sup>34–36</sup> In the fitting of the conventional liquids, the value of  $\beta$  was fixed to 1. The red solid line in Figure 5b is the result of the fit, which reproduces the experimental result quite well. The averaged rotational time  $\langle \tau_{\text{ave}}^r \rangle$  are defined here as

$$\langle \tau_{\text{ave}}^r \rangle = \int_0^\infty \exp(-(t/\tau_s^r)^\beta) dt \quad (12)$$

The parameters obtained by the fit are summarized in Table 2. The averaged reorientational time for each solvent (listed in Table 2) is plotted against the solvent viscosity ( $\eta$ ) in Figure 6.

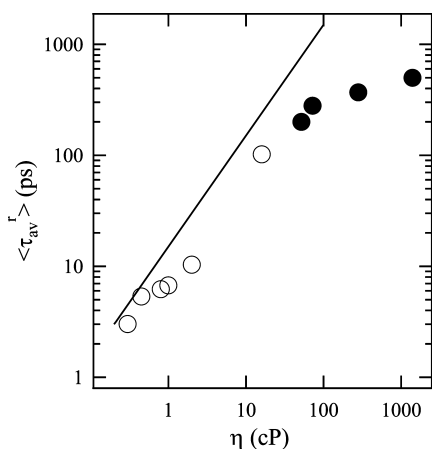


**Figure 6.** Viscosity dependence of average reorientation time in RTILs and molecular liquids. The open and closed symbols represent the ones in molecular liquids and in RTILs, respectively. The solid line is the reorientational time calculated from the SED equation (eqs 13 and 14).

The solid line in the figure is the prediction from the Stokes–Einstein–Debye (SED) equation:<sup>37</sup>

$$\frac{1}{\tau_{\text{calc}}^r} = 6D_{\text{SED}} = \frac{k_B T}{V\eta} \left( \frac{3}{2} \frac{\rho[(2\rho^2 - 1)S - \rho]}{\rho^4 - 1} \right) \quad (13)$$

$$S = (\rho^2 - 1)^{-1/2} \ln[\rho + (\rho^2 - 1)^{1/2}] \quad (14)$$

where  $V$  and  $\rho$  are the solute volume and the axial ratio of solute, respectively. These parameters were taken from the literature (0.04 nm<sup>3</sup> and 1.89 for  $V$  and  $\rho$ , respectively<sup>13a,38,39</sup>). As is shown in the figure, the relaxation times in RTILs are shorter than the prediction from the SED theory.

The deviations from the hydrodynamic theory in RTILs have been often reported for not only rotational diffusion<sup>40,41</sup> but also translational diffusion.<sup>42,43</sup> Several factors have been proposed for the reason for the discrepancy: one is a large void volume of RTILs<sup>40,42</sup> and/or another is the reduced strength of solute–solvent interaction compared to the strong solvent–solvent one in RTILs.<sup>35,43</sup> However, it seems difficult to apply these explanations to the present case because it has been shown that the translational diffusion coefficients of  $I_2^-$  in RTILs apparently obey the hydrodynamic relation.<sup>10</sup> We have to explain the different dependence on the viscosity of the rotational motion from that of the translational motion. In relation with this, the recent study by Yamaguchi et al. is quite suggestive.<sup>44</sup> They measured frequency dependence of the shear viscosity and found that the shear relaxation of RTILs occurs around several hundred MHz (several hundred picoseconds to several nanoseconds). Their result indicates a possibility that the friction acting on the solute molecule is dependent on the time-scale of the motion. For the translational diffusion of  $I_2^-$ , the time-scale (longer than microseconds) is longer than that of the shear relaxation of RTILs, and the bulk viscosity may be a measure of the viscous friction on the translational motion. On the other hand, the rotational relaxation of  $I_2^-$  is similar to or faster than the shear relaxation. As a result, the rotational dynamics of  $I_2^-$  is much faster than the prediction of the SED theory.

**4.3. Coherent Vibration of  $I_2^-$ .** Within 1 ps after the photoexcitation, the time profiles of the absorption show periodic oscillations in conventional liquids.<sup>11a,c,12</sup> One oscillatory component was observed in our transient in ethanol (the black line in Figure 7),

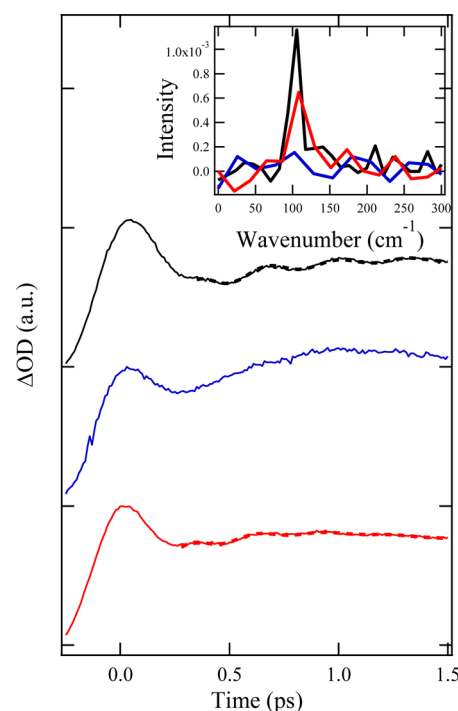


**Figure 7.** Initial time profiles of the transient absorption signals at 880 nm in ethanol (black line), [BMIm][NTf<sub>2</sub>] (blue line) and [BMIm]I (red line). The fitting results with the sin curve (dashed line) are also shown. Each time profile has a different vertical offset for clarity. The inset of figure shows the Fourier transform (FT) spectra of each transient.

as clearly indicated by a Fourier analysis (the inset of the figure), although the oscillatory behavior was not so clear

compared with the previous studies due to broader excitation pulse width of our laser system. This corresponds to the back and forth motion of the  $I_2^-$  wavepacket on the potential surface: The damping oscillation was simulated by  $\exp(-t/\tau_d) \sin(2\pi t \omega_{\text{vib}} + \varphi)$ , where  $\omega_{\text{vib}}$  and  $\tau_d$  represent the frequency of the vibration of  $I_2^-$  and the dephasing time of the oscillation, respectively. The broken lines in Figure 7 show the fitting results, and the parameters obtained by the fit are listed in Table 3. The oscillation frequency and the dephasing time are

**Table 3. Time Constants of Oscillation and Dephasing for Quantum Beats of  $I_2^-$  and  $I_3^-$ <sup>a</sup>**

solvent	$I_2^-$		$I_3^-$	
	$\omega_{\text{vib}}$ (cm <sup>-1</sup> )	$\tau_d$ (ps)	$\omega_{\text{vib}}$ (cm <sup>-1</sup> )	$\tau_d$ (ps)
acetonitrile	102	0.48	110	0.9
methanol	102	0.5	110	0.9
ethanol	102	0.52	110	0.9
1-propanol	102	0.51	110	0.9
water	102	0.5	110	0.8
[BMIm][NTf <sub>2</sub> ]			110	1.2
[BMIm][PF <sub>6</sub> ]			110	1.1
[BMIm][I]	105	0.48	110	1.0
[N <sub>1,1,1,3</sub> ][NTf <sub>2</sub> ]			110	1.1
GTA			110	1.3

<sup>a</sup>In the case of RTILs and high viscosity solvents, the beat of  $I_2^-$  cannot be observed.

very similar among all molecular liquids. On the other hand, the oscillatory behavior was hardly detected in RTILs (see the blue line in Figure 7) and any distinctive component cannot be seen even in the Fourier spectrum of the data (the blue line in the inset figure of Figure 7). The same trend was observed not only for most RTILs but also for high viscosity liquids such as GTA. One plausible reason for the disappearance of the oscillation is the red-shift of the absorption spectrum in RTILs, since the amplitude of the oscillation will be reduced when the probing wavelength gets close to the center of the absorption band. The oscillatory behavior was more visual in probing at the blue or red edge of the absorption band where the absorption changes between on and off resonant prominently according to the position of the wavepacket. However, the oscillation was not detected for the transient at other wavelengths (e.g., 920 nm). On the other hand, a coherent oscillation was detected for [BMIm]I (see the red line of Figure 7 and its FT spectrum), although the amplitude was small. The oscillation frequency and dephasing time (105 cm<sup>-1</sup> and 480 fs) in [BMIm]I were close to those in conventional liquids.

The previous studies reported that the oscillation-amplitude of  $I_2^-$  is affected by the symmetry of the parent ions such as  $I_3^-$  or  $I_2\text{Br}^-$ ,<sup>11c</sup> in the case of  $I_3^-$ , the oscillatory behavior becomes clearer as the symmetry of  $I_3^-$  is broken by solvent, which is evident from the appearance of the forbidden antisymmetric band of  $I_3^-$  (most prominent in ethanol and negligible in acetonitrile).<sup>45</sup> Since the antisymmetric band of  $I_3^-$  is also observed in RTILs as will be shown in Figure 9a, the ground state geometry of  $I_3^-$  in RTILs is deformed by the solvent as in ethanol. Therefore, there is another reason for the disappearance of the coherent vibration of  $I_2^-$ . Another interpretation is the rapid vibrational dephasing due to the high viscosity of RTILs. Several theories predict that the dephasing rate is proportional to  $\eta$  for pure conventional liquids.<sup>46,47</sup> However,

this interpretation contradicts the fact that the coherent vibration is detected for the most viscous [BMIm]I.

One plausible interpretation is the rapid vibrational dephasing of  $I_2^-$  due to the caged-contact pair formation of  $I_2^-$  and I. In the previous paper we have reported that only the caged-contact pair [ $I_2^- \cdots I$ ] is produced after the photodissociation of  $I_3^-$  in viscous liquids and conventional RTILs except for [BMIm]I. We found a good correspondence of the disappearance of the coherent vibration to the formation of the caged contact pair. It is well-known that the vibrational dephasing is accelerated due to the complex formation in the case of hydrogen bonding species( $XH \cdots Y$ ).<sup>48</sup> Robertson and Yarwood explained this by the model in which the intended vibrational mode ( $\nu_{\text{XH}}$ ) loses its coherence by the anharmonic coupling with the stretching mode of hydrogen bond ( $\nu_{\text{XH} \cdots Y}$ ).<sup>48a</sup> Robertson and co-workers also determined the dephasing time of the hydrogen complex between deuterated phenol and dioxin in carbon tetrachloride from the IR absorption band by using this model, and the value is 0.147 ps,<sup>48b</sup> which is much shorter than the case without hydrogen-bonding (more than 1.5 ps<sup>49</sup>). Therefore, it is probable that the dephasing of the caged contact pair [ $I_2^- \cdots I$ ] is too fast for the coherent vibration not to be detected within the time resolution of our system. Further experimental study such as Raman spectra of the contact pair will support this idea.

On the basis of the above idea, we can make some comments on the reaction rate of the photofragment I with solvent  $I^-$  in the case of [BMIm]I. In the previous paper, we reported that free  $I_2^-$  is produced from the reaction of I (the photofragment from  $I_3^-$ ) and the solvent  $I^-$ . This prevents contact pair formation due to the disappearance of I from proximity to  $I_2^-$  and may suppress the acceleration of the dephasing observed in other RTILs. However, for the observation of the coherent vibration of  $I_2^-$ , this reaction should occur while the vibrational coherence is maintained. Since the dephasing time in conventional liquids is ca. 500 fs, the reaction of I with  $I^-$  in the vicinity should occur at least within a few hundred femtoseconds.

The smaller value of the initial anisotropy in [BMIm]I (0.31) compared to the values in ethanol and [BMIm][NTf<sub>2</sub>] (0.36) will support the idea mentioned above. The anisotropy of  $I_2^-$  can be reduced by the additional formation of  $I_2^-$  from I and solvent  $I^-$ . The orientation of the newly formed  $I_2^-$  may not be the same as that of the parent  $I_3^-$  since  $I^-$  can attack I from random directions except for the direction of  $I_2^-$ . Assuming that this reaction produces the completely random-oriented  $I_2^-$ , the initial anisotropy of 0.31 means that one-sixth of the photoproduct I react with the solvent  $I^-$  in an ultrafast time scale.

**4.4. Ground State Dynamics of  $I_3^-$  in [BMIm]I.** The proposed reaction rate of the photoproduct I with the solvent  $I^-$  in [BMIm]I in the previous section is extremely fast for the bimolecular reaction, indicating the complex formation of  $I_3^-$  and  $I^-$  in the ground state. In order to check this possibility, we investigated the ground state dynamics of  $I_3^-$  in [BMIm]I from the ground state bleach recovery observed by 400 nm pump–probe experiment (Figure 8). As reported previously,<sup>11a,12a</sup> a quantum beat of the ground state  $I_3^-$  was observed for the bleach signal in most solvents. The oscillation is attributed to the coherent vibration of  $I_3^-$  wavepacket produced on the ground state potential by the impulsive Raman process. The oscillatory component was analyzed in a similar manner to the  $I_2^-$  vibration, and the values of frequency and dephasing time in

each solvent are listed in Table 3. The vibrational frequency was  $110\text{ cm}^{-1}$  in all solvents, which is consistent with that of the

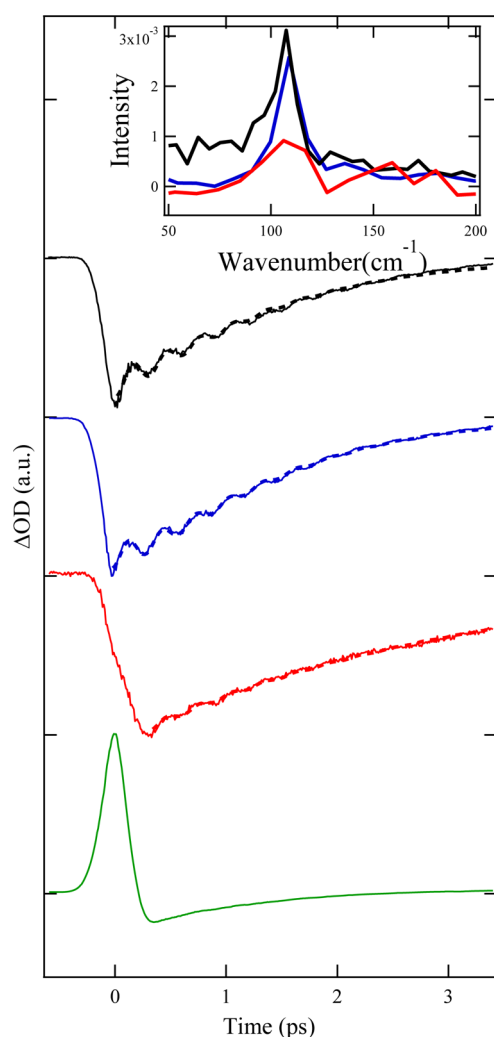


**Figure 8.** Initial time profiles of the transient absorption signals at 400 nm in ethanol (black line), [BMIm][NTf<sub>2</sub>] (blue line), [BMIm]I (red line) and H<sub>2</sub>O with 10 M potassium iodide (green). The fitting results with the sin curve (dashed line) are also shown. Each time profile has a different vertical offset for clarity. The inset of the figure shows the FT spectra of each transient.

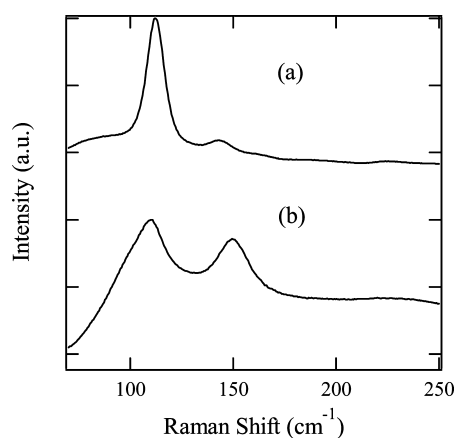


**Figure 9.** Raman spectra in (a) [BMIm][NTf<sub>2</sub>] and (b) [BMIm]I. Each spectrum has a different vertical offset for clarity.

symmetric stretching mode of  $\text{I}_3^-$ . We also carried out a Fourier analysis of these data (the inset of Figure 8). We could not observe other oscillatory components except for the symmetric mode (no observation of antisymmetric mode), different from the previous studies.<sup>12a</sup> This is probably due to the broader excitation pulse width (about 200 fs), which made the weaker vibrations such as the antisymmetric mode invisible.

As is shown in Figure 8, the transient in [BMIm]I is different from other transients mainly in two points: First, the initial rise of the bleach signal is slower in [BMIm]I (red line in Figure 8) in contrast to the pulse-response rise in other solvents (black and blue solid lines in Figure 8). Second the amplitude of the coherent vibration in [BMIm]I is much smaller than other solvents. We consider that the first point is due to the contamination of the two-photon absorption of  $\text{I}^-$ . In Figure 8, we show the transient absorption for the aqueous solution of KI (10 M) without  $\text{I}_3^-$ , which shows a strong photoabsorption (ca. 20 mOD) in the initial stage. Although we could not directly observe the signal of [BMIm]I without  $\text{I}_3^-$  due to the problem of sample preparation, it is considered that a similar extent of the signal contributes to the case of [BMIm]I since the concentration of  $\text{I}^-$  in [BMIm]I is ca. 5 M and the signal intensity was ca. 5 mOD. Therefore, the uniqueness of the  $\text{I}_3^-$  signal in [BMIm]I is the reduced intensity of the coherent vibration. It is probable that  $\text{I}_3^-$  molecules exist in an inhomogeneous environment, and some  $\text{I}_3^-$  molecules interact strongly with  $\text{I}^-$ , which makes the vibrational dephasing of some  $\text{I}_3^-$  molecules fast. This idea is supported in the result of  $\text{I}_3^-$  in aqueous solution with excess of  $\text{I}^-$  (10M), which did not show any beat.

Steady-state Raman spectra of  $\text{I}_3^-$  (Figure 9) also support the ground state interaction between  $\text{I}_3^-$  and  $\text{I}^-$ . In [BMIm][NTf<sub>2</sub>] (Figure 9a), a strong symmetric stretching band ( $110\text{ cm}^{-1}$ ) and a weak antisymmetric stretching band ( $143\text{ cm}^{-1}$ ), which is originally forbidden, are detected as observed for  $\text{I}_3^-$  in conventional molecular liquids. On the other hand, the Raman spectrum of the [BMIm]I (Figure 9b) solution is quite different. Since [BMIm]I was weakly fluorescent when excited at 532 nm probably due to the contamination, there was background rise, which was not well extracted from the presented spectrum. Further, the low frequency region less  $90\text{ cm}^{-1}$  was cut by the edge-filter, and the transition region was somewhat deformed. Therefore, the baseline shift at  $250\text{ cm}^{-1}$  to ca.  $60\text{ cm}^{-1}$  was due to the fluorescence contamination, and it was difficult to compare the absolute signal intensities between the symmetric band ( $110\text{ cm}^{-1}$ ) to the antisymmetric band (ca.  $150\text{ cm}^{-1}$ ). However, it is clear that the antisymmetric band is much stronger than that for [BMIm][NTf<sub>2</sub>]. This indicates that the solvent environment around  $\text{I}_3^-$  is symmetry-broken, i.e.,  $\text{I}_3^-$  is perturbed strongly by  $\text{I}^-$  in the vicinity. Since in RTILs the Coulomb forces between pairs of ions are shielded by the ion-rich environment, ion pairs of the same charge are easier to approach.<sup>10</sup> Therefore, we consider that some portions of  $\text{I}_3^-$  are close to  $\text{I}^-$  in [BMIm]I where numerous  $\text{I}^-$  ions exist, which makes the anomalous ground state dynamics and photodynamics of  $\text{I}_3^-$ .

## 5. CONCLUDING REMARKS

In this work, we investigated VER, rotational relaxation, and vibrational dephasing of  $\text{I}_2^-$  in RTILs after the photodissociation of  $\text{I}_3^-$ . The VER rates in RTILs were slightly slower than those in conventional liquids. On the other hand, the vibrational dephasing was much faster in RTILs. The fast



dephasing was interpreted by the interaction within the caged contact pair. The rotational relaxation showed a nonexponential decay, and the relaxation time was faster than that predicted by the SED theory. The deviation from the SED theory was explained in terms of the frequency dependent friction. [BMIm]I was special for the  $I_3^-$  photodissociation because of the high concentration of  $I^-$ , which caused the fast reaction of the photofragment I. The coherent vibration of  $I_2^-$  and the reduced initial value of anisotropy suggested that the reaction between I and  $I^-$  occurs almost simultaneously with the photodissociation. The ground state dynamics of  $I_3^-$  and steady-state Raman measurement of  $I_3^-$  revealed that there are strong interactions between  $I_3^-$  and  $I^-$ . These results will give important information about the molecular mechanism on the accelerated charge transport for  $I_3^-$  and  $I^-$  in RTILs reported in electrochemical studies. Our results support the exchange mechanism of transport of  $I_3^-$  and  $I^-$  in several ways. First, the ground state complex formation is strongly supported by the Raman and transient absorption measurements. Further, the very fast reaction between  $I^-$  and I suggests the possibility that the charge is transported through the fast chemical reactions in this system. More detailed studies, e.g., concentration dependence of  $I_3^-$  and  $I^-$  will be desirable in the future.

## AUTHOR INFORMATION

### Corresponding Author

\*E-mail: yosi@ims.ac.jp (Y.N.); ykimura@kuchem.kyoto-u.ac.jp (Y.K.).

### Present Address

<sup>†</sup>Department of Photo-Molecular Science, Institute for Molecular Science, Myodaiji, Okazaki 444–8585, Japan.

<sup>‡</sup>Department of Chemical Science and Technology, Faculty of Bioscience and Applied Chemistry, Hosei University, 3-7-2, kajino-cho, koganei, Tokyo 184-8584, Japan.

### Notes

The authors declare no competing financial interest.

## ACKNOWLEDGMENTS

This work is supported by the Grant-in-Aid for Scientific Research (No. 17073012 and No. 23350006) from the Ministry of Education, Culture, Sports, Science, and Technology. Y.N. is supported by the research fellowship for young scientist from JSPS.

## REFERENCES

- (1) *Electrochemical Aspects of Ionic Liquids*; Ohno, H., Ed.; John Wiley & Sons Inc.: Hoboken, NJ, 2005.
- (2) (a) Buzzeo, M. C.; Klymenko, O. V.; Wadhawan, J. D.; Hardacre, C.; Seddon, K. R.; Compton, R. G. *J. Phys. Chem. A* **2003**, *107*, 8872–8878. (b) Evans, R. G.; Klymenko, O. V.; Hardacre, C.; Seddon, K. R.; Compton, R. G. *J. Electroanal. Chem.* **2003**, *556*, 179–188. (c) Evans, R. G.; Klymenko, O. V.; Price, P. D.; Davies, S. G.; Hardacre, C.; Compton, R. G. *Chem. Phys. Chem.* **2005**, *6*, 526–533. (d) Silvester, D. S.; Aldous, L.; Lagunas, M. C.; Hardacre, C.; Compton, R. G. *J. Phys. Chem. B* **2006**, *110*, 22035–22042. (e) Rogers, E. I.; Silvester, D. S.; Jones, S. E.; Aldous, L.; Hardacre, C.; Russell, A. J.; Davies, S. G.; Compton, R. G. *J. Phys. Chem. C* **2007**, *111*, 13957–13966.
- (3) (a) Yamagata, M.; Tachikawa, N.; Katayama, Y.; Miura, T. *Electrochim. Acta* **2007**, *52*, 3317–3322. (b) Tachikawa, N.; Katayama, Y.; Miura, T. *J. Electrochem. Soc.* **2007**, *154*, E211–E216.
- (4) Wang, W.; Balasubramanian, R.; Murray, R. W. *J. Phys. Chem. C* **2008**, *112*, 18207–18216.
- (5) Noda, A.; Susan, M. A. B. H.; Kudo, K.; Mitsushima, S.; Hayamizu, K.; Watanabe, M. *J. Phys. Chem. B* **2003**, *107*, 4024–4033.
- (6) Kawano, R.; Watanabe, M. *Chem. Commun.* **2003**, 330–331.
- (b) Kawano, R.; Watanabe, M. *Chem. Commun.* **2005**, 2107–2109.
- (7) Gratzel, M. *J. Photochem. Photobiol., C: Photochem. Rev.* **2003**, *4*, 145–153.
- (8) (a) Jovanovski, V.; Orel, B.; Jerman, I.; Hočevar, S. B.; Ogorevc, B. *Electrochem. Commun.* **2007**, *9*, 2062–2066. (b) Jerman, I.; Jovanovski, V.; Vuk, A.Š.; Hočevar, S. B.; Gaberšček, M.; Jesih, A.; Orel, B. *Electrochim. Acta* **2008**, *53*, 2281.
- (9) Takahashi, K.; Sakai, S.; Tezuka, H.; Hiejima, Y.; Katsumura, Y.; Watanabe, M. *J. Phys. Chem. B* **2007**, *111*, 4807–4811.
- (10) Nishiyama, Y.; Terazima, M.; Kimura, Y. *J. Phys. Chem. B* **2009**, *113*, 5188–5193.
- (11) (a) Banin, U.; Ruhman, S. *J. Chem. Phys.* **1993**, *98*, 4391. (b) Banin, U.; Kosloff, R.; Ruhman, S. *Chem. Phys.* **1994**, *183*, 289. (c) Gershgoren, E.; Gordon, E.; Ruhman, S. *J. Chem. Phys.* **1997**, *106*, 4806. (d) Gershgoren, E.; Banin, U.; Ruhman, S. *J. Phys. Chem. A* **1998**, *102*, 9. (e) Wang, Z.; Wasserman, T.; Gershgoren, E.; Vala, J.; Kosloff, R.; Ruhman, S. *Chem. Phys. Lett.* **1999**, *313*, 155. (f) Baratz, A.; Ruhman, S. *Chem. Phys. Lett. B* **2008**, *461*, 211–217.
- (12) (a) Kuhne, T.; Vohringer, P. *J. Chem. Phys.* **1996**, *105*, 10788. (b) Kuhne, T.; Vohringer, P. *J. Phys. Chem. A* **1998**, *102*, 4177. (c) Hess, S.; Bürsing, H.; Vohringer, P. *J. Chem. Phys.* **1999**, *111*, 5461.
- (13) (a) Benjamin, I.; Whitnell, R. M. *Chem. Phys. Lett.* **1993**, *204*, 45. (b) Benjamin, I.; Banin, U.; Ruhman, S. *J. Chem. Phys.* **1993**, *98*, 8337. (c) Benjamin, I.; Barbara, P. F.; Gertner, B. J.; Hynes, J. T. *J. Phys. Chem.* **1995**, *99*, 7557.
- (14) Ashkenazi, G.; Banin, U.; Bartana, A.; Kosloff, R.; Ruhman, S. *Adv. Chem. Phys.* **1997**, *100*, 229.
- (15) Harris, C. B.; Smith, D. E.; Russell, D. J. *Chem. Rev.* **1990**, *90*, 481.
- (16) (a) Klinner, D. A. V.; Alfano, J. C.; Barbara, P. F. *J. Chem. Phys.* **1993**, *98*, 5375. (b) Alfano, J. C.; Kimura, Y.; Walhout, P. K.; Barbara, P. F. *Chem. Phys.* **1993**, *175*, 147. (c) Walhout, P. K.; Alfano, J. C.; Thakur, K. A. M.; Barbara, P. F. *J. Phys. Chem.* **1995**, *99*, 7568.
- (17) Nishiyama, Y.; Terazima, M.; Kimura, Y. *Chem. Phys. Lett. B* **2010**, *491*, 164–168.
- (18) Fujisawa, T.; Fukuda, M.; Terazima, M.; Kimura, Y. *J. Phys. Chem. A* **2006**, *110*, 6164.
- (19) Chen, E. C. M.; Wentworth, W. E. *J. Phys. Chem.* **1985**, *89*, 4099.
- (20) Condon, E. U. *Phys. Rev.* **1928**, *32*, 858.
- (21) Winans, J. G.; Stueckelberg, E. C. G. *Proc. Natl. Acad. Sci. U.S.A.* **1928**, *14*, 867.
- (22) Stueckelberg, E. C. G. *Phys. Rev.* **1932**, *42*, 518.
- (23) Gislason, E. A. J. *Chem. Phys.* **1973**, *58*, 3702.
- (24) Tripathi, G. N. R.; Schuler, R. H.; Fessenden, R. W. *Chem. Phys. Lett.* **1985**, *113*, 563–568.
- (25) Owrutsky, J. C.; Raftery, D.; Hochstrasser, R. M. *Annu. Rev. Phys. Chem.* **1994**, *45*, 519.
- (26) Dahl, K.; Sando, G. M.; Fox, D. M.; Sutto, T. E.; Owrutsky, J. C. *J. Chem. Phys.* **2005**, *123*, 084504.
- (27) Sando, G. M.; Dahl, K.; Owrutsky, J. C. *Chem. Phys. Lett.* **2006**, *418*, 402.
- (28) Shim, Y.; Kim, H. J. *J. Chem. Phys.* **2006**, *125*, 024507.
- (29) Grote, R. F.; Hynes, J. T. *J. Chem. Phys.* **1982**, *77*, 3736.
- (30) Whitnell, R. M.; Wilson, K. R.; Hynes, J. T. *J. Phys. Chem.* **1990**, *94*, 8625–8628.
- (31) Ladanyi, B. M.; Stratt, R. M. *J. Chem. Phys.* **1999**, *111*, 2008–2018.
- (32) Gnanakaran, S.; Hochstrasser, R. M. *J. Chem. Phys.* **1996**, *105*, 3486.
- (33) Bagchi, B.; Biswas, R. *Adv. Chem. Phys.* **1999**, *109*, 207–433.
- (34) (a) Ito, N.; Arzhantsev, S.; Heitz, M.; Maroncelli, M. *J. Phys. Chem. B* **2004**, *108*, 5771. (b) Jin, H.; Baker, G. A.; Arzhantsev, S.; Dong, J.; Maroncelli, M. *J. Phys. Chem. B* **2007**, *111*, 7291. (c) Jin, H.; Li, X.; Maroncelli, M. *J. Phys. Chem. B* **2007**, *111*, 13473.
- (35) Dutt, G. B. *J. Phys. Chem. B* **2010**, *114*, 8971.
- (36) Funston, A. M.; Fadeeva, T. A.; Wishart, J. F.; Castner, E. W. *J. Phys. Chem. B* **2007**, *111*, 4963.

- (37) Fleming, G. R. *Chemical Applications of Ultrafast Spectroscopy*; Oxford University Press: New York, 1986.
- (38) Tasker, P. W.; Balint-Kurti, G. G.; Dixon, R. N. *Mol. Phys.* **1976**, *32*, 1651–1660.
- (39) Borsarelli, C. D.; Bertolotti, S. G.; Previtali, C. M. *Photochem. Photobiol. Sci.* **2003**, *2*, 791–795.
- (40) (a) Miyake, Y.; Hidemori, T.; Akai, N.; Kawai, A.; Shibuya, K.; Koguchi, S.; Kitazume, T. *Chem. Lett.* **2009**, *38*, 124. (b) Miyake, Y.; Akai, N.; Kawai, A.; Shibuya, K. *J. Phys. Chem. A* **2011**, *115*, 6347.
- (41) Mali, K. S.; Dutt, G. B.; Mukherjee, T. *J. Chem. Phys.* **2005**, *123*, 174504.
- (42) (a) Morgan, D.; Ferguson, L.; Scovazzo, P. *Ind. Eng. Chem. Res.* **2005**, *44*, 4815–4823. (b) Ferguson, L.; Scovazzo, P. *Ind. Eng. Chem. Res.* **2007**, *46*, 1369–1374.
- (43) Nishiyama, Y.; Fukuda, M.; Terazima, M.; Kimura, Y. *J. Chem. Phys.* **2008**, *128*, 164514.
- (44) Yamaguchi, T.; Miyake, S.; Koda, S. *J. Phys. Chem. B* **2010**, *114*, 8126.
- (45) Johnson, A. E.; Myers, A. J. *J. Phys. Chem.* **1996**, *100*, 7778.
- (46) Oxtoby, D. W. *J. Chem. Phys.* **1979**, *70*, 2605–2610.
- (47) Oxtoby, D. W. *J. Chem. Phys.* **1979**, *70*, 2605–2610.
- (48) (a) Robertson, G. N.; Yarwood, J. *J. Chem. Phys.* **1978**, *32*, 267. (b) Yarwood, J.; Ackroyd, R.; Robertson, G. N. *J. Chem. Phys.* **1978**, *32*, 283–299.
- (49) Stone, P. J.; Thompson, H. W. *Spectrochim. Acta* **1957**, *10*, 17.